ACS chemical biology

Articles

pubs.acs.org/acschemicalbiology

Substrate/Product-Targeted NMR Monitoring of Pyrimidine Catabolism and Its Inhibition by a Clinical Drug

Hisatsugu Yamada,[†] Keigo Mizusawa,[‡] Ryuji Igarashi,[§] Hidehito Tochio,[§] Masahiro Shirakawa,[§] Yasuhiko Tabata,[¶] Yu Kimura,[†] Teruyuki Kondo,[†] Yasuhiro Aoyama,*[,⊥] and Shinsuke Sando*[,∥]

[†]Advanced Biomedical Engineering Research Unit, Kyoto University, Katsura, Nishikyo-ku, Kyoto 615-8510, Japan

[‡]Department of Synthetic Chemistry and Biological Chemistry and [§]Department of Molecular Engineering, Graduate School of Engineering, Kyoto University, Katsura, Nishikyo-ku, Kyoto 615-8510, Japan

[¶]Department of Biomaterials, Field of Tissue Engineering, Institute for Frontier Medical Sciences, Kyoto University, 53 Kawara-cho Shogoin, Sakyo-ku, Kyoto 606-8507, Japan

[⊥]Department of Molecular Chemistry and Biochemistry, Faculty of Science and Engineering, Doshisha University, Kyotanabe, Kyoto 610-0321, Japan

[∥] INAMORI Frontier Research Center, Kyushu University, 744 Motooka, Nishi-ku, Fukuoka 819-0395, Japan

S *Supporting Information*

ABSTRACT: We report the application of one-dimensional triple-resonance NMR to metabolic analysis and thereon-based evaluation of drug activity. Doubly $^{13}C/^{15}N$-labeled uracil ($[^{15}N1,^{13}C6]$-uracil) was prepared. Its catabolic (degradative) conversion to $[^{13}C3,^{15}N4]$-β-alanine and inhibition thereof by gimeracil, a clinical co-drug used with the antitumor agent 5-fluorouracil, in mouse liver lysates were monitored specifically using one-dimensional triple-resonance ($^{1}H-\{^{13}C-^{15}N\}$) NMR, but not double-resonance ($^{1}H-\{^{13}C\}$) NMR, in a ratiometric manner. The administration of labeled uracil to a mouse resulted in its non-selective distribution in various organs, with efficient catabolism to labeled β-alanine exclusively in the liver. The co-administration of gimeracil inhibited the catabolic conversion of uracil in the liver. In marked contrast to *in vitro* results, however, gimeracil had practically no effect on the level of uracil in the liver. The potentiality of triple-resonance NMR in the analysis of *in vivo* pharmaceutical activity of drugs targeting particular metabolic reactions is discussed.

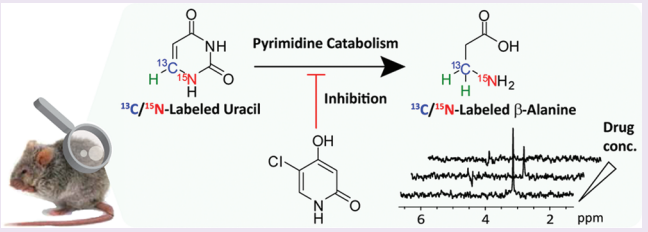

The cell is a complex system composed of various molecules and diverse metabolic reactions. *In situ* monitoring of a particular cellular reaction remains a challenge. NMR spectroscopy has great potential in this regard. It is applicable to any biomolecule with selectivity and sensitivity, depending on the types of measurement employed.[1−3] High selectivity is an essential requirement for further *ex vivo* or *in vivo* applications, especially for molecule-targeted NMR imaging (MRI). Where applicable, ^{19}F NMR using ^{19}F-labeled substrates/inhibitors,[4−6] in combination with signal off-on techniques,[7−10] turns out to be a powerful tool. Otherwise, the use of $^{13}C/^{15}N$-enriched probes as *real* substrates in combination with a multiple-resonance technique is a promising approach.[3,11−20] Multiple-resonance NMR uses magnetic coherence transfer between spin-coupled nuclei. Therefore, it can be used to measure the ^{13}C-bound proton ($^{1}H-^{13}C$) selectively (double resonance).[3,11−15] In cases where the ^{13}C atom is further bound to ^{15}N ($^{1}H-^{13}C-^{15}N$), the proton involved would be detected more selectively under triple-resonance conditions,[16−21] as it can be defined more specifically on the HCN basis (triple resonance) than on the HC basis (double resonance).

We focused on one-dimensional (1D) triple-resonance NMR, which is termed triple-resonance isotope-edited (TRIED) NMR.[17−20] This is a method that correlates three successive NMR-active nuclei with different Larmor frequencies ($^{1}H-^{13}C-^{15}N$ in the present case).[21] The pulse scheme may be so optimized on the basis of a predetermined chemical shift and coupling-constant data that magnetic coherence transfers *via* spin−spin scalar coupling from ^{1}H through ^{13}C to ^{15}N and then back through ^{13}C to ^{1}H, which allows selective detection of the proton in the particular $^{1}H-^{13}C-^{15}N$ sequence of the probe. This is the theme of this work; with its future application to molecule-targeted MRI in mind, we focus here on selective or independent detection of a particular molecule using optimized pulse conditions. This technique, which is applicable, in principle, to various HCN compounds, should markedly suppress background noise, as the probability of natural occurrence of this connectivity ($^{1}H-^{13}C-^{15}N$) is as low as 0.0040% (the natural abundance of ^{13}C and ^{15}N is 1.1% and

Received: September 27, 2011
Accepted: January 4, 2012
Published: January 19, 2012

   dx.doi.org/10.1021/cb2003972 | *ACS Chem. Biol.* 2012, 7, 535−542

0.37%, respectively). In addition, 1D triple resonance is much simpler and less time-consuming than the multidimensional (*e.g.*, 3D, 4D) triple resonance that is used widely in the structural analysis of [^{13}C,^{15}N]-labeled proteins, which generally requires hours or days for data acquisition. Thus, 1D triple-resonance NMR may provide a powerful and practical tool for the detection and monitoring of probes labeled appropriately with isotopes [^{13}C,^{15}N]; it is also applicable to metabolic analysis, although examples of the latter remain limited.[17−19] In this context, the analysis of disease-related metabolic disorders is an intriguing area of research. The *in situ* evaluation of the activity of drugs that are supposed to inhibit a particular metabolic reaction is another avenue of research. To the best of our knowledge, this is the first report of an example of the latter approach.

We applied the 1D ^{1}H−{^{13}C−^{15}N} triple-resonance technique to the catabolic analysis of pyrimidine bases using doubly labeled [^{15}N1,^{13}C6]-uracil as a probe. The metabolism of uracil (and of other pyrimidine bases) comprises anabolic and catabolic pathways (for uracil (R = H) and 5-fluorouracil (R = F) in Figure 1).[22,23] The anabolic/catabolic activities are

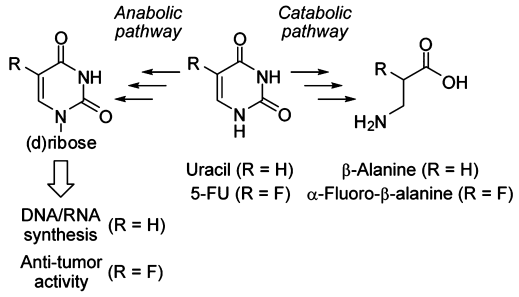

Figure 1. Outline of uracil metabolism. Anabolic and catabolic pathways of uracil (R = H) and 5-fluorouracil (5-FU) (R = F).

closely linked to the efficacy of pyrimidine-related drugs, such as 5-fluorouracil (5-FU), which is a tumor chemotherapeutic agent.[24] A part of the 5-FU administered is anabolically converted to 5-fluoro-(2′-deoxy)uridine monophosphate, which exerts an antitumor activity, *e.g.*, by inhibiting thymidylate synthase, an enzyme that is essential for the growth of tumors.[25,26] The remaining 5-FU (∼80%) undergoes prompt degradation to α-fluoro-β-alanine along the catabolic pathway.[24,27] It has been suggested that the drug efficacy of 5-FU can be improved by the co-administration of inhibitors that block the catabolic (degradation) pathway, thus resulting in a temporal increase in the concentration of 5-FU.[28−31] However, there is also an indication that deficiency in this catabolic activity causes a pharmacogenetic disorder,[32] suggesting that the toxic side effects of 5-FU can be diminished by its catabolic degradation.[33] Prediction of side effects is a matter of importance in chemotherapy of cancer and related diseases. For this purpose, a breath test (for $^{13}CO_2$ in exhaled breath; in reference to the scheme shown in Figure 2A) for 2-^{13}C-labeled uracil-administrated patients has been developed.[34] Under these circumstances, we were prompted to develop a direct analytical method for pyrimidine catabolism. This is how we started the present work. Here, we report that (1) the conversion of uracil to β-alanine (in tissue lysates or in live mice) can be monitored specifically using the 1D triple-resonance NMR technique and that (2) gimeracil, which is a clinical drug, inhibits this conversion both *in vitro* and *in vivo*, albeit in different ways.

RESULTS AND DISCUSSION

Labeled Uracil, Labeled β-Alanine, and Their 1D ^{1}H−{^{13}C−^{15}N} Triple-Resonance NMR Spectra. Figure 2A shows the established catabolic pathway of uracil. It undergoes three successive enzymatic reactions: reduction of uracil to give 5,6-dihydrouracil, hydrolytic cleavage of the amide (imide) N3−C4 bond to afford β-ureidopropionate, and conversion of the latter into the final catabolite, β-alanine, with concomitant release of CO_2 and NH_3. Throughout the whole pathway, the H−C6−N1 linkage (colored in Figure 2), which is the site of double labeling (^{13}C and ^{15}N), remains intact. On the basis of the reasonable assumption that isotope labeling does not alter the catabolic pathway dramatically, one could expect doubly labeled [^{15}N1,^{13}C6]-uracil to give rise to doubly labeled [^{13}C3,^{15}N4]-β-alanine as the final product. Both uracil and β-alanine possess a ^{1}H−^{13}C−^{15}N linkage, but their chemical features are different in terms of chemical shift and spin−spin coupling. In uracil, the hydrogen in question is bound to the olefinic carbon, which in turn is bound to amide nitrogen. Conversely, β-alanine is an aliphatic (saturated) amine. Thus, we expected that the starting material (uracil) and its end product (β-alanine), which constitute the uracil catabolic pathway, could be monitored using 1D ^{1}H−{^{13}C−^{15}N} triple-resonance NMR, not only selectively but also separately. This is because magnetic coherence transfer between ^{1}H and ^{13}C and ^{13}C and ^{15}N is mediated by spin−spin scalar coupling, which implies that the pulse parameters can be optimized to be specific to the proton in a particular ^{1}H−^{13}C−^{15}N sequence. This was the case (see below).

Doubly labeled [^{15}N1,^{13}C6]-uracil (hereafter termed labeled uracil) was prepared from ethyl *N*-(2-cyanoacetyl)carbamate in three steps[35] (Figure 2B), using labeled triethyl orthoformate ($H^{13}C(OCH_2CH_3)_3$) and labeled ammonium chloride ($^{15}NH_4Cl$) as sources of ^{13}C and ^{15}N, respectively. 1D ^{1}H−{^{13}C−^{15}N} triple-resonance NMR spectra were obtained using an INEPT-like pulse sequence (Supplementary Figure S1). The 1D triple-resonance NMR for labeled uracil in D_2O showed a single ^{1}H peak (Figure 2C, top) at 7.44 ppm for the **^{1}H**−^{13}C−^{15}N moiety, when the pulse sequence was optimized particularly for that moiety using relevant chemical-shift and coupling-constant data (^{13}C = 143 ppm, ^{15}N = 110 ppm, J_{C-H} = 184 Hz, and J_{C-N} = 7.7 Hz). In a similar manner, the corresponding ^{1}H signal for the **$^{1}H_2$**−^{13}C−^{15}N moiety in [$^{13}C_3$,^{15}N]-β-alanine, which was used as an authentic specimen for labeled β-alanine, was detected at 3.09 ppm also as a single peak when using β-alanine-optimized parameters (^{13}C = 36.3 ppm, ^{15}N = 30.5 ppm, J_{C-H} = 145 Hz, and J_{C-N} = 5.2 Hz) (Figure 2D, top). Under uracil-optimized pulse conditions, labeled β-alanine was completely NMR silent (Figure 2D, bottom). Similarly, labeled uracil was completely NMR inactive under β-alanine-optimized pulse conditions (Figure 2C, bottom). Therefore, the detection of the substrate and product of uracil catabolism can be rendered independent using respectively optimized pulse conditions.

***In Situ* Monitoring of Uracil Catabolism and Its Inhibition in a Tissue Lysate.** First, we monitored the conversion of uracil to β-alanine in a mouse liver lysate. Labeled uracil (0.5 mM) was incubated at 37 °C with a crude liver lysate (10% v/v) containing β-NADPH (2 mM, a cofactor of

dx.doi.org/10.1021/cb2003972 | ACS Chem. Biol. 2012, 7, 535−542

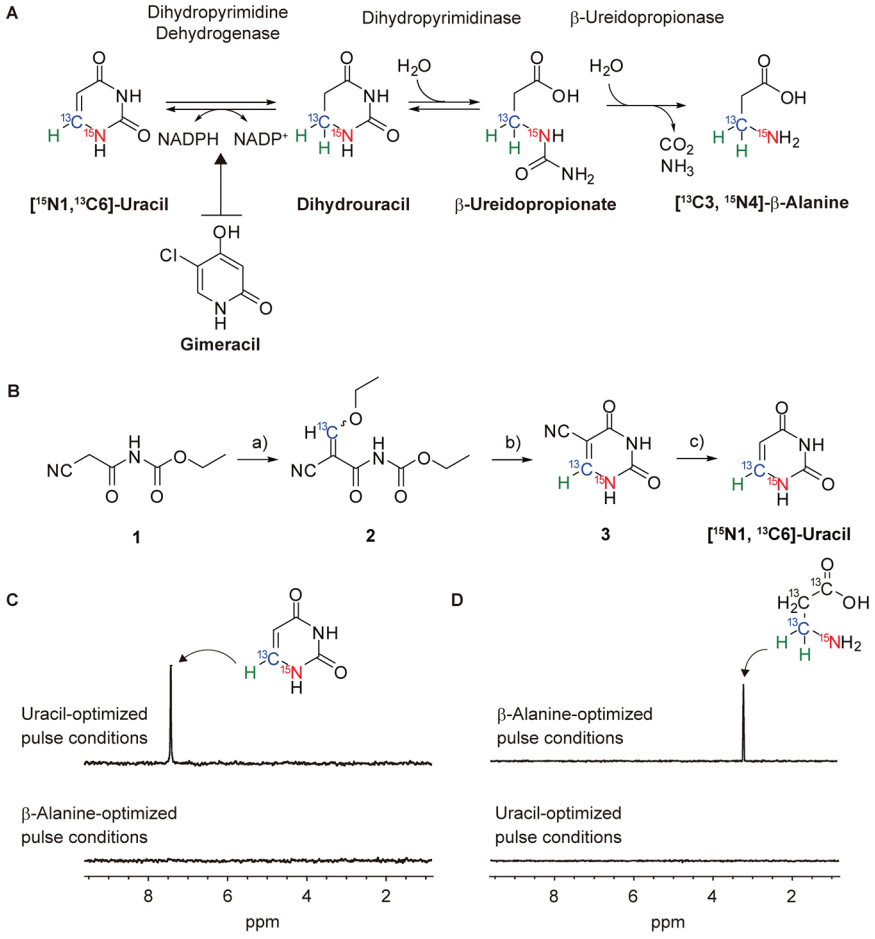

Figure 2. Labeled uracil, labeled *β*-alanine, and their 1D $^{1}H-\{^{13}C-^{15}N\}$ triple-resonance NMR spectra. (A) Catabolic degradation of labeled uracil to give labeled *β*-alanine (target $^{1}H-^{13}C-^{15}N$ sequences are colored). Gimeracil (5-chloro-4-hydroxy-2-pyridone), which was used as an inhibitor of the first (dihydropyrimidine dehydrogenase) reaction, is also shown. (B) Preparation of [$^{15}N1$,$^{13}C6$]-labeled uracil. Reagents and conditions: (a) labeled triethyl orthoformate ($H^{13}C(OCH_2CH_3)_3$), acetic anhydride, reflux, 7 h, 86%; (b) labeled ammonium chloride ($^{15}NH_4Cl$), aqueous NaOH, reflux, 5 h, 93%; (c) aqueous HCl, reflux, 27 h, 95%. (C) 1D triple-resonance NMR spectra of [$^{15}N1$,$^{13}C6$]-labeled uracil (1 mM) in D_2O under uracil-optimized (top) and *β*-alanine-optimized (bottom) pulse conditions. (D) 1D triple-resonance NMR spectra of [$^{13}C_3$,^{15}N]-labeled *β*-alanine (0.66 mM) in D_2O under *β*-alanine-optimized (top) and uracil-optimized (bottom) pulse conditions. Spectra were obtained after 64 scans.

dihydropyrimidine dehydrogenase). After 1 h, the mixture was lyophilized, redissolved in D_2O, and subjected to NMR analysis. The results are shown in Figure 3. The conventional (single-resonance) ^{1}H NMR spectrum (Figure 3A) was completely useless; all NMR-active molecules in the lysate contributed to the spectrum. The 1D $^{1}H-\{^{13}C\}$ double-resonance spectrum (Figure 3B), obtained using appropriately *β*-alanine-optimized pulse conditions (a 2D HSQC pulse sequence modified for the 1D ^{1}H experiments and chemical-shift (^{13}C = 36.3 ppm) and coupling-constant data (J_{C-H} = 145 Hz)), was composed of many (>20) signals, indicating that 1D double resonance is far from satisfactory in suppressing background noise (the 1D $^{1}H-\{^{13}C\}$ double-resonance spectrum obtained using uracil-optimized pulse conditions is shown as Figure S10 in the Supporting Information). The 1D triple-resonance spectrum obtained using *β*-alanine-optimized pulse conditions (Figure 3C, top) exhibited a single peak at 3.09 ppm, which was assignable to the $^{1}H_2-^{13}C-^{15}N$ signal of [$^{13}C3$,$^{15}N4$]-*β*-alanine, as confirmed independently using 2D $^{1}H-^{13}C$ HSQC analysis. Under uracil-optimized conditions, there appeared only a trace amount of the corresponding $^{1}H-^{13}C-^{15}N$ signal at 7.44 ppm for labeled uracil (Figure 3C, bottom). The yield of *β*-alanine was ≥80% (~0.41 mM). In the absence of liver lysate, uracil remained as such (Figure 3D, top, uracil-optimized conditions), and no signal was detected for *β*-alanine (Figure 3D, bottom, *β*-alanine-optimized conditions). These results indicate clearly that the otherwise stable uracil undergoes complete catabolic conversion to *β*-alanine in a liver lysate using the conditions described here and that both the substrate and the product can be monitored selectively and separately using the triple-resonance ($^{1}H-\{^{13}C-^{15}N\}$), but not the double-resonance ($^{1}H-\{^{13}C\}$), technique. Control experiments showed that a concentration of labeled probe ≥4.5 *μ*M in a crude liver lysate can be detected with a good signal-to-noise ratio >3 using our triple-resonance conditions (256 scans).

We then moved on to check the effect of an inhibitor of the catabolic conversion of uracil. Gimeracil (5-chloro-4-hydroxy-2-pyridone) was the inhibitor of choice here (Figure 2A). It is used clinically in combination with pyrimidine-type antitumor agents, such as 5-FU.[28,29] The supposed pharmaceutical role of gimeracil is the inhibition of the dihydropyrimidine dehydrogenase reaction, which is the first step of uracil catabolism (Figure 2A), thus preventing the catabolic degradation of the antitumor drug.[23,24] The inhibitory effects of increasing amounts of gimeracil were monitored by following either labeled *β*-alanine or labeled uracil under conditions that were

dx.doi.org/10.1021/cb2003972 | ACS Chem. Biol. 2012, 7, 535–542

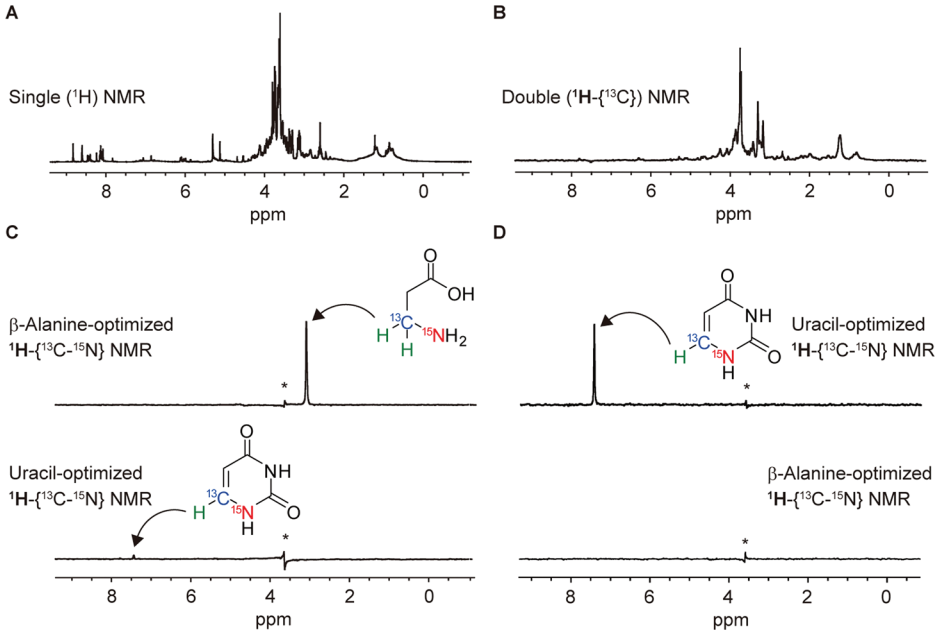

Figure 3. NMR analysis of the catabolic conversion of uracil to β-alanine in a crude liver lysate. Single-resonance ^{1}H NMR (A), 1D ^{1}H−{^{13}C} double-resonance NMR (B), and 1D ^{1}H−{^{13}C−^{15}N} triple-resonance NMR (C, under β-alanine-optimized (top) or uracil-optimized (bottom) conditions) spectra of a mouse liver lysate (10% v/v) containing [^{15}N1,^{13}C6]-labeled uracil (0.5 mM) in 10 mM Tris-HCl (pH 8.0), 0.5 mM EDTA, 0.5 mM 2-mercaptoethanol, 2 mM dithiothreitol, 5 mM $MgCl_2$, and 2 mM NADPH, incubated at 37 °C for 1 h. (D) Uracil-optimized (top) and β-alanine-optimized (bottom) 1D triple-resonance NMR spectra in the absence of liver lysate under conditions that were otherwise identical to those described above. Single-resonance (panel A), double-resonance (panel B), and triple-resonance (panels C and D) spectra were obtained after 32, 256, and 256 scans, respectively. The symbol * denotes a noise derived from the buffer solution.

otherwise identical to those described above ([labeled uracil] = 0.5 mM and 1 h of incubation). The results of these experiments (Figure 4A, [β-alanine] produced, measured under β-alanine-optimized pulse conditions; and Figure 4B, [labeled uracil] remaining, measured under uracil-optimized conditions) were consistent with each other. Gimeracil at lower concentrations (<16 nM = 1.6×10^{-8} M) had little effect on the conversion of uracil to β-alanine. At higher concentrations, it inhibited the conversion in a [gimeracil]-dependent manner, until reaching maximal or complete inhibition at around 50 μM (5×10^{-5} M), where [inhibitor]/[substrate] = gimeracil/uracil = 0.1. A good mass-balance between uracil and β-alanine indicates that the anabolic activity of the present lysate system is relatively low.

Monitoring of Uracil Catabolism and Its Inhibition in a Mouse. We then analyzed the catabolism of uracil in a live mouse. Labeled uracil (300 μg g^{-1} = 2.6 μmol g^{-1} body weight) was administered intraperitoneally to a mouse bearing murine colon adenocarcinoma C-26 inoculated subcutaneously. After 1 h, tissues (tumor, blood, liver, kidney, heart, and small intestine) were collected, lysed, redissolved in D_2O, and subjected to 1D triple-resonance NMR analysis of the product (β-alanine) and substrate (uracil) using β-alanine-optimized and uracil-optimized pulse conditions, respectively, as described above. The results are shown in Figure 5A and B, respectively, where signal intensities are weight-normalized for each organ. As shown in Figure 5B, uracil was detected in every tissue, whereas the signal intensity in the liver was significantly lower than those observed in other organs.

Accordingly, the formation of β-alanine was detected conspicuously in the liver; the corresponding signal intensities were of a noise (background) level in the tumor, blood, heart, and small intestine and barely detectable in the kidney (Figure

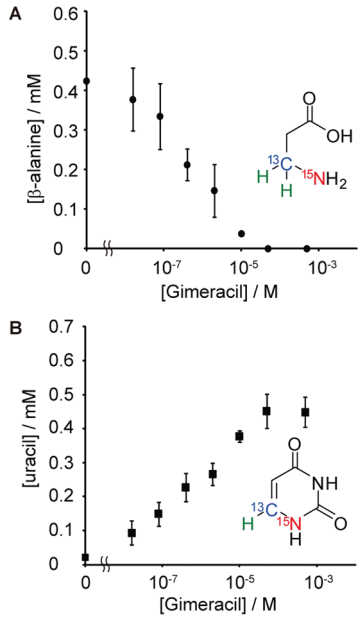

Figure 4. Inhibitory effects of gimeracil on the catabolic conversion of uracil to β-alanine in a crude liver lysate. The amount of β-alanine produced (A, under β-alanine-optimized conditions) and the amount of uracil remaining (B, under uracil-optimized conditions) in the presence of varying amounts (0−0.5 mM) of gimeracil in a crude liver lysate under conditions that were otherwise identical to those described in Figure 3 ([labeled uracil] = 0.5 mM, 1 h of incubation at 37 °C and 256 scans). The concentrations of β-alanine and uracil were quantified *via* calibration of the corresponding NMR peak integrals using authentic samples. Error bars represent the standard deviation of three independent measurements.

dx.doi.org/10.1021/cb2003972 | *ACS Chem. Biol.* 2012, 7, 535−542

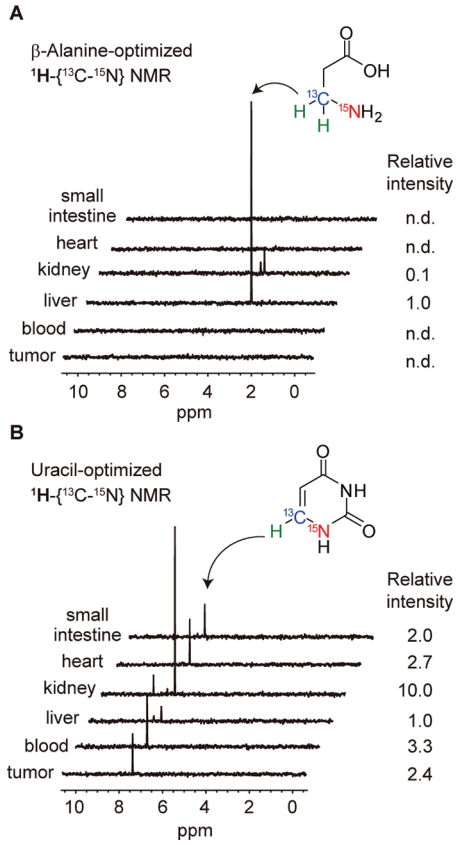

Figure 5. 1D triple-resonance NMR analysis of the catabolic conversion of uracil to β-alanine in a mouse. Spectra, weight-normalized for each organ, obtained under β-alanine-optimized (A) and uracil-optimized (B) conditions for the extracts from tumor (murine colon adenocarcinoma, colon-26), blood (200 μL), liver, kidney, heart, and small intestine of a mouse injected intraperitoneally with a solution of [^{15}N1,^{13}C6]-labeled uracil (300 μg g^{-1} body weight). Relative intensities shown are peak integrals of the β-alanine (A) or uracil (B) signals for various organs relative to that for the liver as a standard (1.0). "n.d." indicates that the signal intensity is too low to allow evaluation of the accurate numerical value.

5A). These results indicate clearly that uracil is distributed non-selectively in various organs and that uracil undergoes efficient catabolic degradation to β-alanine exclusively in the liver.

In addition to the major peaks of β-alanine and uracil, three minor peaks were also observed in Figure 5. The 2D ^{1}H−^{13}C HSQC analyses (Supplementary Figures S11−S13) revealed that the minor peaks at 3.28 ppm (kidney, Figure 5A) and 7.72 ppm (just detectable amount in liver, kidney, and small intestine, Figure 5B) are assigned to β-ureidopropionate (catabolic intermediate, referring to Figure 2A) and (deoxy)-uridine/thymidine or (deoxy)uridine/thymidine phosphate (anabolic intermediate, referring to Figure 1), respectively. Detection of ureidopropionate only in kidney may be consistent with the fact that kidney has a considerably diminished (as compared with liver) ureidopropionase activity.[36] Detection of a nucleoside/nucleotide derivative indicates that uracil indeed undergoes anabolism in these organs. The third minor peak at 8.34 ppm (kidney, Figure 5B) might be assigned to purine nucleotide, although we have to be very careful about this speculation since uracil-to-purine conversion has not been demonstrated.

For comparison, we took the mass (ESI-TOF) spectrum (both positive and negative modes) for the labeled uracil-treated liver sample. The results were terrible, the spectrum being composed of many unidentified peaks with no detectable one for uracil or β-alanine. Clearly, the performance of mass spectroscopy at least for the present "admixture" sample is no comparison with the present NMR method.

Our final concern pertained to how gimeracil works in the liver of a live mouse. Various amounts of gimeracil (0.023−2.3 μmol g^{-1} body weight) were co-administered with a constant amount of labeled uracil (263 μg g^{-1} = 2.3 μmol g^{-1} body weight) to a mouse. After 1 h, the liver was dissected, treated as described above and subjected to 1D triple-resonance NMR analysis. Gimeracil acted as an inhibitor of the conversion of uracil to β-alanine. As shown in Figure 6A and B (blue bars),

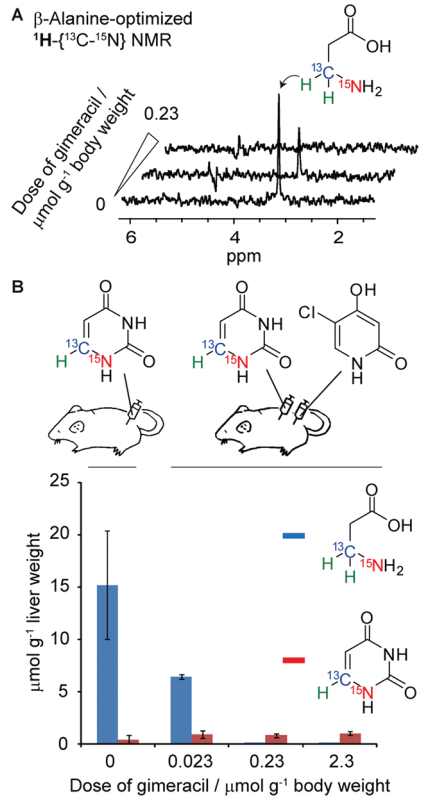

Figure 6. Effects of gimeracil on the catabolic conversion of uracil to β-alanine in mice. (A) 1D triple-resonance NMR spectra (weight normalized) obtained using β-alanine-optimized conditions for the extracts of liver of mice injected intraperitoneally with varying amounts (0−2.3 μmol g^{-1} body weight) of gimeracil, together with a constant amount (2.3 μmol g^{-1} body weight) of [^{15}N1,^{13}C6]-labeled uracil. (B) The amount of [^{13}C3,^{15}N4]-labeled β-alanine produced (blue bars, obtained using β-alanine-optimized conditions) and of uracil remaining (red bars, obtained using uracil-optimized conditions) in the extracts of the liver of mice co-injected with labeled uracil and gimeracil (0−2.3 μmol g^{-1}). The concentrations of β-alanine and uracil were quantified *via* calibration of the corresponding NMR peak integrals using authentic samples. Error bars represent the standard deviation of three independent measurements.

the amount of β-alanine formed (15 ± 5 μmol g^{-1} liver weight, corresponding to ∼30% of the total dose of uracil administered in the absence of gimeracil) decreased with increasing doses of gimeracil, and complete inhibition occurred at 0.23 μmol g^{-1} for gimeracil, *i.e.*, at an inhibitor/substrate (gimeracil/uracil)

dx.doi.org/10.1021/cb2003972 | *ACS Chem. Biol.* 2012, 7, 535−542

ratio of 0.1. This was in accordance with the result described above using the *in vitro* system (isolated liver lysate). Notably, however, inhibition of the formation of β-alanine was not accompanied by an increase in the amount of intact uracil. Irrespective of the presence (0.023, 0.23, or 2.3 μmol g^{-1} body weight) or absence of gimeracil, the amount of uracil in the liver was kept at a constant low level ($\leq$1.0 μmol g^{-1} liver weight) (Figure 6B, red bars). This was in marked contrast to the results of the *in vitro* system (isolated liver tissue; Figure 4), in which gimeracil inhibited the conversion of uracil to β-alanine clearly, thereby increasing or recovering the in-tissue uracil level. It might be reasonable to interpret the *in vivo* results in terms of anabolic or salvage activity; the excess amount of uracil induced by gimeracil in the live liver may undergo rapid anabolism (salvage) to leave only a small and steady amount of intact uracil. In this context, the present results may be in accord with the suggested pharmaceutical role of gimeracil as a clinical drug. While analysis of the uracil-treated mouse liver in the presence or absence of gimeracil shows just detectable, at best (Figure 5B), amounts of pyrimidine anabolites such as (deoxy)uridine/thymidine and (deoxy)uridine/thymidine phosphate, in contrast to the 5-fluorouracil case,[31] this is not surprising if we make a reasonable assumption that the anabolic (salvage) pathway for *natural* uracil is rapid *in vivo*. It is not surprising either that the uridine/thymidine moieties in the resulting RNA/DNA are rendered NMR-silent because of rapid relaxation of high-molecular-weight biopolymers.

Another possible explanation is to suppose that gimeracil induces redistribution of uracil. Indeed, uracil in the liver of mice, either gimeracil-treated or -untreated, is kept constant at a low level (Figures 5B and 6B) as if suggesting that there is some sort of distribution "equilibrium", and hence redistribution in a gimeracil-treated mouse, among various organs for uracil to keep its level low in the liver . If this is the case, the apparently discrepant *in vitro* results (Figure 4) become self-evident; the catabolism-inhibited uracil in the liver lysates in the presence of gimeracil simply remains as such, because there is no other organ to be redistributed in. The two mechanisms (anabolic pathway and redistribution) may operate simultaneously, although we defer full interpretation until we get a deeper insight into pharmacokinetics of uracil in mice. Whatever the mechanism may be, the apparent contrast between the *in vitro* (isolated mouse liver tissue) and *in vivo* (liver of a live mouse) results strongly suggests the significance of direct evaluation of pharmaceutical effects under *in vivo* condition. In summary, the high specificity of 1D ^{1}H–{^{13}C–^{15}N} triple-resonance NMR demonstrated here provides a sound basis for analysis of *in vivo* (in animal) metabolic events and thereon-based evaluation of drug activities.

Conclusion. The present work demonstrated the potential utility of 1D triple-resonance (^{1}H–{^{13}C–^{15}N} in this case) NMR for metabolic analysis. By choosing optimized pulse parameters based on predetermined chemical-shift and coupling-constant data, one can target particular **^{1}H–^{13}C–^{15}N** protons almost completely free from noise signals; this high selectivity cannot be achieved using 1D single- (**^{1}H**) or double-resonance (**^{1}H–{^{13}C}**) NMR, which even when applicable requires careful distinction of the target ^{1}H signals from the background emanating from the endogenous biomolecules. Thus, 1D triple-resonance NMR allows the specific monitoring of both the decay of the substrate and the growth of the product, selectively and separately in a ratiometric manner. This high selectivity is an essential requirement in application to molecule-targeted ^{1}H NMR imaging of a particular metabolite. In this context, we may have opened a door to a new phase of MRI.

By applying the present technique to the catabolic analysis of uracil, we confirmed that (1) uracil undergoes degradation to β-alanine in the liver, both *in vitro* and *in vivo*, and (2) gimeracil inhibits this conversion *in vitro* and *in vivo*, with (*in vitro*) or without (*in vivo*) concomitant increase in the level of uracil. Gimeracil, which is a clinical drug, had apparently no effect on the level of uracil in the liver of a mouse treated with uracil. Rigorous identification of the fate of catabolism-inhibited uracil remains a subject for further research. The present technique would advance our understanding of the role of co-drug, not only gimeracil against 5-FU but also many other known ones.

From a more general point of view, it emphasizes the importance of the evaluation of *in vivo* activity of a drug that targets a particular metabolic reaction, and the present method's potential for that purpose. As compared with other sensitive analytical tools such as ^{19}F NMR, mass spectrometry, and antibody-based detection, the present method has a fascinating potential of being applicable to non-invasive detection of small metabolites (and other small biomarkers) of real biotransformations using real, although ^{13}C,^{15}N-labeled, substrates. In the drug discovery area, it may even open the door to *in vivo* screening of drugs.

Various types of metabolic reactions of pharmaceutical interest use relatively simple CHN compounds as substrates. The introduction of ^{13}C and ^{15}N into this type of substrate usually requires laborious preparative work. However, the probe obtained from it is a real substrate, although the possible effects of the isotopes (^{13}C versus ^{12}C and ^{15}N versus ^{14}N) on rates and equilibria should always be taken into account. The utility of uniformly ^{13}C/^{15}N-labeled probes, which are more readily available than the regiospecifically labeled ones, should also be kept in mind.[37] Further work along these lines is currently under way in our laboratories.

METHODS

General. Labeled uracil ([^{15}N1,^{13}C6]-uracil) was prepared using three steps starting from ethyl *N*-(2-cyanoacetyl)carbamate (Figure 2B), as detailed in the Supporting Information. Commercially available [$^{13}C_3$,^{15}N]-β-alanine (99% isotope purity for both ^{13}C and ^{15}N) (ISOTEC) was used as an authentic specimen for labeled β-alanine.

All 1D ^{1}H–{^{13}C–^{15}N} triple-resonance NMR spectra were recorded at 298 K on a Bruker Avance 700 spectrometer equipped with a 5 mm TCI CryoProbe, using an INEPT-like pulse sequence (Supplementary Figure S1). The parameters used for the detection of ^{1}H–^{13}C–^{15}N in labeled uracil were transmitter offsets of ^{13}C = 143 ppm and ^{15}N = 110 ppm and delay intervals of $1/4^{1}J_{CH}$ = 1.36 ms and $1/4^{1}J_{CN}$ = 32 ms. Those used for the detection of ^{1}H–^{13}C–^{15}N in labeled β-alanine were ^{13}C = 36.3 ppm, ^{15}N = 30.5 ppm, $1/4^{1}J_{CH}$ = 1.72 ms, and $1/4^{1}J_{CN}$ = 48 ms. The size of the FID was 2,048 complex points, and the spectral width was 11,261.26 Hz with an acquisition time of 90.98 ms. The FID obtained was apodized using an exponential window function with the line broadening parameter lb =10 Hz. Data processing and analysis were performed using the Topspin 1.3 (Bruker Biospin) program. The concentrations of labeled uracil and β-alanine produced were quantified using authentic samples in reference to the calibration line of triple-resonance peak integrals plotted against known amounts of the authentic specimen under the same NMR conditions. All animal experiments were performed according to the Institutional Guidance of Kyoto University on Animal Experimentation and under permission by the animal experiment committee of Faculty of Engineering, Kyoto University.

dx.doi.org/10.1021/cb2003972 | *ACS Chem. Biol.* 2012, 7, 535–542

Catabolic Conversion of Uracil to β-Alanine in a Mouse Liver Lysate. The liver tissues of female C57BL/6J mice (Shimizu Laboratory Supplies Co. Ltd.) weighing ∼15 g were harvested and homogenized (1:2, w/v) in a 20 mM Tris-HCl (pH 8.0) solution containing 1 mM EDTA and 1 mM 2-mercaptoethanol, using a Qiagen TissueLyser. The homogenate was then centrifuged at 25,000*g* for 1 h at 4 °C. The supernatant fluid was collected and used as the liver lysate. The enzymatic reactions were performed in an aqueous solution containing 10 mM Tris-HCl (pH 8.0), 0.5 mM EDTA, 0.5 mM 2-mercaptoethanol, 2 mM dithiothreitol, 5 mM $MgCl_2$, 2 mM NADPH, 0.5 mM [^{15}N1,^{13}C6]-labeled uracil, 0−0.5 mM gimeracil, and 10% (v/v) liver lysate. After incubation at 37 °C for 1 h, the reaction mixtures were lyophilized to dryness, dissolved in D_2O (500 μL), and subjected to NMR analysis (256 scans, ∼7 min).

Catabolic Conversion of Uracil to β-Alanine in Mice. Female BALB/cCrSlc mice (Shimizu Laboratory Supplies Co. Ltd.) weighing ∼13 g were used. Animals were inoculated subcutaneously with 1.0×10^7 cells of colon 26 in the left hind limb 10 days prior to the experiments. A tumor-bearing mouse was injected intraperitoneally with an aqueous solution of [^{15}N1,^{13}C6]-uracil (300 μg g^{-1} = 2.6 μmol g^{-1} body weight) in PBS. The mouse was sacrificed by an overdose inhalation of anesthetic 1 h after the administration of labeled uracil. Tissues (tumor, blood, liver, kidney, heart, and small intestine) were harvested and homogenized in a 5-fold weight of 10% trichloroacetic acid (TCA) using a Qiagen TissueLyser. After incubation for 30 min on ice, the homogenates were centrifuged at 12,000 rpm for 5 min at RT and the aqueous extracts were collected. The residues were washed with a 5-fold weight of 10% TCA, and the extracts were collected after centrifugation. The combined aqueous extracts were lyophilized to dryness and dissolved in the same amount of D_2O as the weight of each tissue, for weight normalization of signal intensities. After centrifugation (13,200 rpm for 30 min), 70 μL of the supernatant, containing extracts derived from 70 mg of tissue, was taken for NMR analysis (1,024 scans, ∼30 min).

Evaluation of the Inhibitory Effects of Gimeracil in Mice. Female BALB/cCrSlc mice weighing ∼13 g were injected intraperitoneally with a solution of [^{15}N1,^{13}C6]-labeled uracil (2.3 μmol g^{-1} body weight) and gimeracil (0, 0.023, 0.23, and 2.3 μmol g^{-1}). The mouse was sacrificed by an overdose inhalation of anesthetic 1 h after the administration of labeled uracil. According to the protocol described above, the whole liver was harvested, homogenized and extracted using 10% TCA. The aqueous extracts were lyophilized to dryness and dissolved in the same amount of D_2O as the weight of the liver tissue (∼620 mg). After centrifugation (13,200 rpm for 30 min), 70 μL of the supernatant, containing extracts derived from 70 mg of the tissue, was taken for NMR analysis (256 scans, ∼7 min).

■ ASSOCIATED CONTENT

Supporting Information

Preparation of labeled uracil, pulse scheme for 1D ^{1}H−{^{13}C−^{15}N} triple-resonance NMR, NMR spectra for labeled compounds, uracil-optimized 1D HSQC spectrum, and 2D HSQC spectra. This material is available free of charge *via* the Internet at http://pubs.acs.org.

■ AUTHOR INFORMATION

Corresponding Author

*E-mail: (S.S.) ssando@ifrc.kyushu-u.ac.jp; (Y.A) yaoyama@mail.doshisha.ac.jp .

■ ACKNOWLEDGMENTS

This research was supported financially by the Innovative Techno-Hub for Integrated Medical Bio-imaging Project of the Special Coordination Funds for Promoting Science and Technology from MEXT, Japan and by the NEXT Program and Grants-in-Aid No. 22685018 and 20655037 from JSPS, Japan.

■ REFERENCES

(1) Griffin, J. L. (2003) Metabolomics: NMR spectroscopy and pattern recognition analysis of body fluids and tissues for characterization of xenobiotic toxicity and disease diagnosis. *Curr. Opin. Chem. Biol. 7*, 648−654.

(2) Glunde, K., Artemov, D., Penet, M., Jacobs, M. A., and Bhujwalla, Z. M. (2010) Magnetic resonance spectroscopy in metabolic and molecular imaging and diagnosis of cancer. *Chem. Rev. 110*, 3043−3059.

(3) Fan, T., and Lane, A. (2008) Structure-based profiling of metabolites and isotopomers by NMR. *Prog. Nucl. Magn. Reson. Spectrosc. 52*, 69−117 and references therein.

(4) Cobb, S. L., and Murphy, C. D. (2009) ^{19}F NMR application in chemical biology. *J. Fluor. Chem. 130*, 132−143 and references therein.

(5) Yu, J.-x., Kodibagkar, V. D., Cui, W., and Mason, R. P. (2005) ^{19}F: A versatile reporter for non-invasive physiology and pharmacology using magnetic resonance. *Curr. Med. Chem. 12*, 819−848.

(6) van Laarhoven, H. W. M., Punt, C. J. A., Kamm, Y. J. L., and Heerschap, A. (2005) Monitoring fluoropyrimidine metabolism in solid tumors with *in vivo* ^{19}F magnetic resonance spectroscopy. *Crit. Rev. Oncol. Hematol. 56*, 321−343.

(7) Mizukami, S., Takikawa, R., Sugihara, F., Hori, Y., Tochio, H., Wälchli., M., Shirakawa, M., and Kikuchi, K. (2008) Paramagnetic relaxation-based ^{19}F MRI probe to detect protease activity. *J. Am. Chem. Soc. 130*, 794−795.

(8) Takaoka, Y., Sakamoto, T., Tsukiji, S., Narazaki, M., Matsuda, T., Tochio, H., Shirakawa, M., and Hamachi, I. (2009) Self-assembling nanoprobes that display off/on ^{19}F nuclear magnetic resonance signals for protein detection and imaging. *Nat. Chem. 1*, 557−561.

(9) Langereis, S., Keupp, J., van Velthoven, J. L. J., de Roos, I. H. C., Burdinski, D., Pikkemaat, J. A., and Grüll, H. (2009) A temperature-sensitive liposomal ^{1}H CEST and ^{19}F contrast agent for MR image-guided drug delivery. *J. Am. Chem. Soc. 131*, 1380−1381.

(10) Tanaka, K., Kitamura, N., Takahashi, Y., and Chujo, Y. (2009) Reversible signal regulation system of ^{19}F NMR by redox reactions using a metal complex as a switching module. *Bioorg. Med. Chem. 17*, 3818−3823.

(11) Forseth, R. R., and Shoroeder, F. C. (2011) NMR-spectroscopic analysis of mixtures: from structure to function. *Curr. Opin. Chem. Biol. 15*, 38−47.

(12) Rothman, D. L., Behar, K. L., Hetherington, H. P., Hollander, A. D., Bendall, M. R., Petroff, O. A. C., and Shulman, R. G. (1985) ^{1}H-Observe/^{13}C-decouple spectroscopic measurements of lactate and glutamate in the rat brain *in vivo*. *Proc. Natl. Acad. Sci. U.S.A. 82*, 1633−1637.

(13) van Zijl, P. C. M., Scott Chesnick, A., DesPres, D., Moonen, C. T. W., Ruiz-Cabello, J., and van Gelderen, P. (1993) *In Vivo* proton spectroscopy and spectroscopic imaging of {1-^{13}C}-glucose and its metabolic products. *Magn. Reson. Med. 30*, 544−551.

(14) de Graaf, R. A., Mason, G. F., Patel, A. B., Behar, K. L., and Rothman, D. L. (2003) *In vivo* ^{1}H-[^{13}C]-NMR spectroscopy of cerebral metabolism. *NMR Biomed. 16*, 339−359.

(15) Kato, Y., Okollie, B., and Artemov, D. (2006) Noninvasive ^{1}H/^{13}C magnetic resonance spectroscopic imaging of the intratumoral distribution of Temozolomide. *Magn. Res. Med. 55*, 755−761.

(16) Chikayama, E., Suto, M., Nishihara, T., Shinozaki, K., and Kikuchi, J. (2008) Systematic NMR analysis of stable isotope labeled metabolite mixtures in plant and animal systems: Coarse grained views of metabolic pathways. *PLoS ONE 3*, e3805 and references therein.

(17) Hutton, W. C., Likos, J. J., Gard, J. K., and Garbow, J. R. (1998) Triple resonance isotope-edited (TRIED): a powerful new NMR technique for studying metabolism. *J. Labelled Compd. Radiopharm. 41*, 87−95.

(18) Gard, J. K., Feng, P. C. C., and Hutton, W. C. (1997) Nuclear magnetic resonance time course studies of glyphosate metabolism by microbial soil isolates. *Xenobiotica 27*, 633−644.

(19) Mizusawa, K., Igarashi, R., Uehira, K., Takafuji, Y., Tabata, Y., Tochio, H., Shirakawa, M., Sando, S., and Aoyama, Y. (2010) Turn-on

detection of targeted biochemical reactions by triple resonance NMR analysis using isotope-labeled probe. *Chem. Lett. 39*, 926−928.
(20) Yamaguchi, K., Ueki, R., Yamada, H., Aoyama, Y., Nonaka, H., and Sando, S. (2011) In situ analysis of [8-^{13}C-7-^{15}N]-double-labelled theophylline by triple resonance NMR technique. *Anal. Methods 3*, 1664−1666.
(21) Kay, L. E., Ikura, M., Tschudin, R., and Bax, A. (1990) Three-dimensional triple resonance NMR spectroscopy of isotopically enriched proteins. *J. Magn. Reson. 89*, 496−514.
(22) Traut, T. W., and Loechel, S. (1984) Pyrimidine catabolism: individual characterization of the three sequential enzymes with a new assay. *Biochemistry 23*, 2533−2539.
(23) Naguib, F. N. M., el Kouni, M. H., and Cha, S. (1985) Enzymes of uracil catabolism in normal and neoplastic human tissues. *Cancer Res. 45*, 5405−5412.
(24) Longley, D. B., Harkin, D. P., and Johnston, P. G. (2003) 5-Fluorouracil: mechanisms of action and clinical strategies. *Nat. Rev. Cancer 3*, 330−338.
(25) Schwartz, E. L., Baptiste, N., Wadler, S., and Makower, D. (1995) Thymidine phosphorylase mediates the sensitivity of human colon-carcinoma cells to 5-fluorouracil. *J. Biol. Chem. 270*, 19073−19077.
(26) Evrard, A., Cuq, P., Robert, B., Vian, L., Pelegrin, A., and Cano, J. P. (1999) Enhancement of 5-fluorouracil cytotoxicity by human thymidine-phosphorylase expression in cancer cells: *In vitro* and *in vivo* study. *Int. J. Cancer 80*, 465−470.
(27) Heggie, G. D., Sommadossi, J.-P., Cross, D. S., Huster, W. J., and Diasio, R. B. (1987) Clinical pharmacokinetics of 5-fluorouracil and its metabolites in plasma, urine, and bile. *Cancer Res. 47*, 2203−2206.
(28) Hirasaka, T., Nakano, K., Takeuchi, T., Satake, H., Uchida, J., Fujioka, A., Saito, H., Okabe, H., Oyama, K., Takeda, S., Unemi, N., and Fukushima, M. (1996) Antitumor activity of 1 M tegafur-0.4 M 5-chloro-2, 4-dihydroxypyridine-1 M potassium oxonate (S-1) against human colon carcinoma orthotopically implanted into nude rats. *Cancer Res. 56*, 2602−2606.
(29) Takechi, T., Fujioka, A., Matsushima, E., and Fukushima, M. (2002) Enhancement of the antitumor activity of 5-fluorouracil (5-FU) by inhibiting dihydropyrimidine dehydrogenase activity (DPD) using 5-chloro-2,4-dihydroxypyridine (CDHP) in human tumor cells. *Eur. J. Cancer 38*, 1271−1277.
(30) Inoue, S., Ohtani, H., Tsujimoto, M., Hori, S., and Sawada, Y. (2007) Development of a pharmacokinetic model to optimize the dosage regimen of TS-1, a combination preparation of tegafur, gimeracil and oteracil potassium. *Drug Metab. Pharmacokinet. 22*, 162−168.
(31) Adams, E. R., Leffert, J. J., Craig, D. J., Spector, T., and Pizzorno, G. (1999) *In vivo* effect of 5-ethynyluracil on 5-fluorouracil metabolism determined by ^{19}F nuclear magnetic resonance spectroscopy. *Cancer Res. 59*, 122−127.
(32) van Kuilenburg, A. B. P., Haasjes, J., Richel, D. J., Zoetekouw, L., Van Lenthe, H., De Abreu, R. A., Maring, J. G., Vreken, P., and van Gennip, A. H. (2000) Clinical implications of dihydropyrimidine dehydrogenase (DPD) deficiency in patients with severe 5-fluorouracil-associated toxicity: Identification of new mutations in the DPD gene. *Clin. Cancer Res. 6*, 4705−4712.
(33) Johnson, M. R., and Diasio, R. B. (2001) Importance of dihydropyrimidine dehydrogenase (DPD) deficiency in patients exhibiting toxicity following treatment with 5-fluorouracil. *Adv. Enzyme Regul. 41*, 151−157.
(34) Mattison, L. K., Ezzeldin, H., Carpenter, M., Modak, A., Johnson, M. R., and Diasio, R. B. (2004) Rapid identification of dihydropyrimidine dehydrogenase deficiency by using a novel 2-^{13}C-uracil breath test. *Clin. Cancer Res. 10*, 2652−2658.
(35) Kaminski, V. V., Comber, R. N., Wexler, A. J., and Swenton, J. S. (1983) Anion-mediated fragmentation reactions. Mechanistic and synthetic aspects of the fragmentation and rearrangement reactions of pyrimidinedione-alkyne photoadducts. *J. Org. Chem. 48*, 2337−2346.
(36) Tamaki, N., Mizutani, N., Kikugawa, M., Fujimoto, S., and Mizota, C. (1987) Purification and properties of β-ureidopropionase from the rat liver. *Eur. J. Biochem. 169*, 21−26.
(37) Amini, S. K., Shaghaghi, H., Bain, A. D., Chabok, A., and Tafazzoli, M. (2010) Magnetic resonance tensors in Uracil: Caluculation of ^{13}C, ^{15}N, ^{17}O NMR chemical shifts, ^{17}O and ^{14}N electric field gradients and measurement of ^{13}C and ^{15}N chemical shifts. *Solid State NMR 37*, 13−20.